Quality Improvement Study

Medicine®

OPEN

Metal artifacts reduction in computed tomography: A phantom study to compare the effectiveness of metal artifact reduction algorithm, model-based iterative reconstruction, and virtual monochromatic imaging

Takuya Ishikawa, MD, PhD, Shigeru Suzuki, MD, PhD*, Shingo Harashima, RT, Rika Fukui, RT, Masafumi Kaiume, MD, Yoshiaki Katada, MD, PhD

Abstract

The purpose of this study was to compare the effectiveness of a metal artifact reduction algorithm (MAR), model-based iterative reconstruction (MBIR), and virtual monochromatic imaging (VMI) for reducing metal artifacts in CT imaging.

A phantom study was performed for quantitatively evaluating the dark bands and fine streak artifacts generated by unilateral hip prostheses. Images were obtained by conventional scanning at 120 kilovolt peak, and reconstructed using filtered back projection, MAR, and MBIR. Furthermore, virtual monochromatic images (VMIs) at 70 kilo-electron volts (keV) and 140 keV with/without use of MAR were obtained by dual-energy CT. The extents and mean CT values of the dark bands and the differences in the standard deviations and location parameters of the fine streak artifacts evaluated by the Gumbel method in the images obtained by each of the methods were statistically compared by analyses of variance.

Significant reduction of the extent of the dark bands was observed in the images reconstructed using MAR than in those not reconstructed using MAR (all, $P < .01$). Images obtained by VMI at 70 keV and 140 keV with use of MAR showed significantly increased mean CT values of the dark bands as compared to those obtained by reconstructions without use of MAR (all, $<.01$). Significant reduction of the difference in the standard deviations used to evaluate fine streak artifacts was observed in each of the image sets obtained with VMI at 140 keV with/without MAR and conventional CT with MBIR as compared to the images obtained using other methods (all, $P < .05$), except between VMI at 140 keV without MAR and conventional CT with MAR. The location parameter to evaluate fine streak artifacts was significantly reduced in CT images obtained using MBIR and in images obtained by VMI at 140 keV with/without MAR as compared to those obtained using other reconstruction methods (all, $P < .01$).

In our present study, MAR appeared to be the most effective reconstruction method for reducing dark bands in CT images, and MBIR and VMI at 140 keV appeared to the most effective for reducing streak artifacts.

Abbreviations: CT = computed tomography, FBP = filtered back projection, keV = kilo-electron volts, kVp = kilovolt peak, MAR = metal artifact reduction, MBIR = model-based iterative reconstruction, ROI = region of interest, SD = standard deviation, VMI = virtual monochromatic imaging.

Keywords: computed tomography, metal artifact reduction, metal artifacts, model-based iterative reconstruction, virtual monochromatic imaging

Editor: Ismaheel Lawal.

The authors report no conflicts of interest.

The datasets generated during and/or analyzed during the current study are available from the corresponding author on reasonable request.

Department of Radiology, Tokyo Women's Medical University Medical Center East, 2-1-10 Nishiogu, Arakawa-ku, Tokyo, Japan.

** Correspondence: Shigeru Suzuki, Department of Radiology, Tokyo Women's Medical University Medical Center East, 2-1-10 Nishiogu, Arakawa-ku, Tokyo 116-8567, Japan (e-mail: shig.suz@gmail.com).*

How to cite this article: Ishikawa T, Suzuki S, Harashima S, Fukui R, Kaiume M, Katada Y. Metal artifacts reduction in computed tomography: A phantom study to compare the effectiveness of metal artifact reduction algorithm, model-based iterative reconstruction, and virtual monochromatic imaging. Medicine 2020;99:50 (e23692).

Received: 21 July 2020 / Received in final form: 19 October 2020 / Accepted: 14 November 2020

http://dx.doi.org/10.1097/MD.0000000000023692

1. Introduction

Since the advent of computed tomography (CT), metal artifacts caused by metal implants such as coils, stents, dental fillings, and orthopedic hardware have posed significant problems interfering with the diagnostic accuracy, and the issue remains challenging. The presence of artifacts makes it difficult to evaluate not only the implants themselves, but also implant-bone interface and other adjacent structures.[1,2]

Metal artifacts manifest in various forms. They could manifest as thick and band-shaped low attenuation areas (dark bands) arising from metal implants, sometimes accompanied by white bands,[3] or as thin lines alternately appearing dark and bright (fine streak artifacts) generated around the metal implants.[4]

Previous studies have demonstrated the effectiveness of various reconstruction techniques used in clinical practice in reducing metal artifacts, such as metal artifact reduction algorithms (MARs), model-based iterative reconstruction (MBIR), and virtual monochromatic imaging (VMI).[5–11]

However, there have been no reports that have classified metal artifacts into dark bands and fine streak artifacts, and compared the effectiveness of each of the 3 reconstruction methods. Thus, the purpose of the study was to initially compare the efficacy of these techniques in reducing the dark bands and fine streak artifacts in a phantom study using a hip prosthesis.

2. Materials and methods

2.1. Phantom and metal implant

The custom phantom was made with a unilateral hip prosthesis (Fig. 1), which consists of the shell made of titanium with an outer diameter of 56 mm, the liner made of ultra-high-molecular-weight polyethylene with an inner diameter of 40 mm, the head made of zirconia- reinforced alumina with an outer diameter of 40 mm, the adaptor sleeve made of titanium, and the stem made of titanium with a length of 126 mm (Striker Orthopedics, Mahwah, NJ, US). The unilateral hip prosthesis was inserted into a cylindrical container made of polyethylene with a diameter of 290 mm and height of 330 mm. We fixed the stem with Styrofoam, and then fixed it in a water-filled container. A phantom filled with water, without the hip prosthesis, was also constructed. Ethical approval was not necessary, because this was a phantom study.

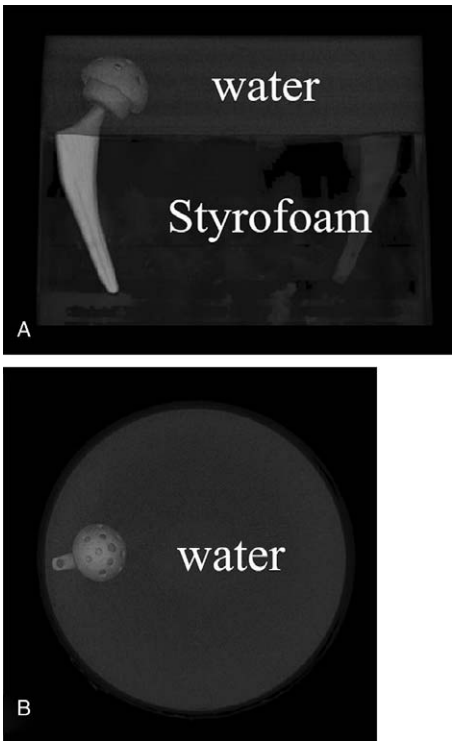

Figure 1. Volume rendering image of the phantom (A, B). The phantom with a unilateral hip prosthesis made of titanium was prepared and images from axial scanning were obtained. The images that included the artificial head were utilized for the analyses.

2.2. Image acquisition and reconstruction

CT imaging of the phantoms was performed with the Discovery CT750 HD system (GE Healthcare, Milwaukee, WI, US). The phantom was placed with its central axis overlapping the axis of the gantry. Images were obtained by conventional scanning at a 120 kilovolt peak (kVp) using the following parameters: tube current, 700 mA; collimation, 64×0.625 mm; pitch, 0.984; gantry rotation, 0.4 seconds; scan field of view, 50 cm. The CTDIvol was 22.82 mGy. The images were reconstructed at 0.625 mm thickness and intervals with a standard reconstruction kernel. Then, the images were further reconstructed by filtered back projection (FBP), use of MAR (GE Healthcare), and MBIR (Veo 3.0; GE Healthcare). Furthermore, dual-energy CT was performed with fast kilovoltage switching of 80 and 140 kVp. The scanning conditions were the same as those mentioned above, except for the following parameters: tube current, 600 mA; pitch, 1.375; gantry rotation, 1.0 second. The CTDIvol was 23.28 mGy. The reconstructed images were transferred to a workstation (Advantage Workstation version 4.6; GE Healthcare), and the gemstone spectral imaging application was applied to the images obtained in the dual-energy scan mode to generate VMIs at 70 kilo-electron volts (keV) and 140 keV using/not using MAR. For each condition, the image with the largest cross-sectional area of the artificial head (center slice) was selected from the obtained images, and a total of 21 slices (center slice, and 10 slices each above and below the center slice) were utilized for quantitative analyses with the MATLAB software (Mathworks, Natrick, MA, US). For the case of the phantom without the hip prosthesis, 21 slices in the same range were evaluated.

2.3. Evaluation of dark bands

We placed a region of interest (ROI) at the center (water part) of the image reconstructed by FBP and measured the CT values: the standard deviation (SD) was 24.13 Hounsfield unit. We set −3 SD (−72.4 Hounsfield unit) as the threshold for dark bands and defined dark bands as low attenuation areas whose CT values were less than the threshold. Pixels with CT values less than the threshold were detected within ROI 1 with a diameter of 280 mm, excluding ROI 2 with a diameter of 47 mm placed at the head to exclude the unnatural low attenuation area that occurs near the artificial head (Fig. 2). Then, the extent and mean CT values of the dark bands were calculated on the 21 images obtained under each imaging/reconstruction condition.

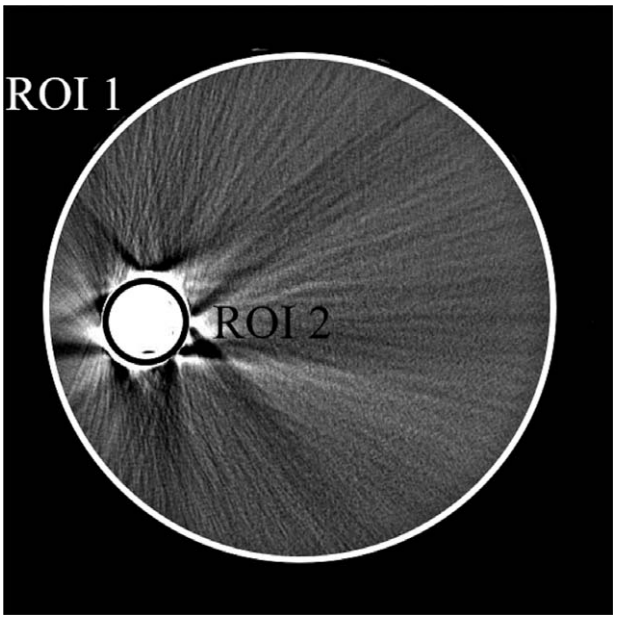

Figure 2. For the assessment of dark bands, pixels with computed tomography values of less than the threshold within ROI 1, excluding ROI 2, were detected. ROI = region of interest.

2.4. Evaluation of fine streak artifacts

Fine streak artifacts were defined as thin, alternately appearing dark and bright lines. Differences in the SDs and location parameters calculated by the Gumbel method were utilized for the assessment of the fine streak artifacts. As for the differences in the SDs, an ROI that is circular in shape and 30 mm in diameter was placed on the side opposite to the hip prosthesis where no dark bands seemed to appear in the phantom with the metal implant (Fig. 3A). An ROI was also set in the same area in the phantom without the metal implant (Fig. 3B). The SD of the CT values within the ROI in the phantom without the metal implant was subtracted from that in the phantom with the metal implant. Then, the difference in the SD was calculated in the 21 images obtained under each imaging/reconstruction condition.

2.5. Gumbel method to assess fine streak artifacts

In this study, we evaluated fine streak artifacts using the Gumbel method devised by Imai et al.[12,13] The method is based on the principle that variations of the CT attenuation caused by fine streak artifacts can be statistically modeled by the Gumbel distribution. In brief, the largest difference between adjacent CT numbers of one CT number profile is attributed to fine streak artifacts.[12,13]

A rectangular ROI measuring 40 pixels in width and 100 pixels in length was placed almost perpendicular to the fine streak artifacts on the opposite side of the hip prosthesis where no dark bands seemed to appear (Fig. 4A). Forty parallel-line profiles measuring 100 pixels in length were placed and the CT values were measured (Fig. 4B). The largest difference between adjacent CT values was obtained for each of the CT number profiles. Then, the Gumbel distribution was analyzed, as follows:

$$F(x) = \exp\{-\exp[-(x-\beta)/\gamma]\}$$

where β and γ are the location and scale parameters, respectively, the location parameter to the mode of that distribution and the scale parameter to its variance.[12,13] Then, the unknown cumulative probability function was also estimated using the mean rank method, which was expressed as:

$$F(xi) = 1/(n+1)$$

for i=1, . . . , n,

where n denotes the sampling size (in this study, $n=40$), and $x_1 \leq x_2 \ldots \leq x_{40}$ denote the 40 arranged differences.[12,13] When the fitting line for the Gumbel plot was expressed as:

$$\gamma = ax + b$$

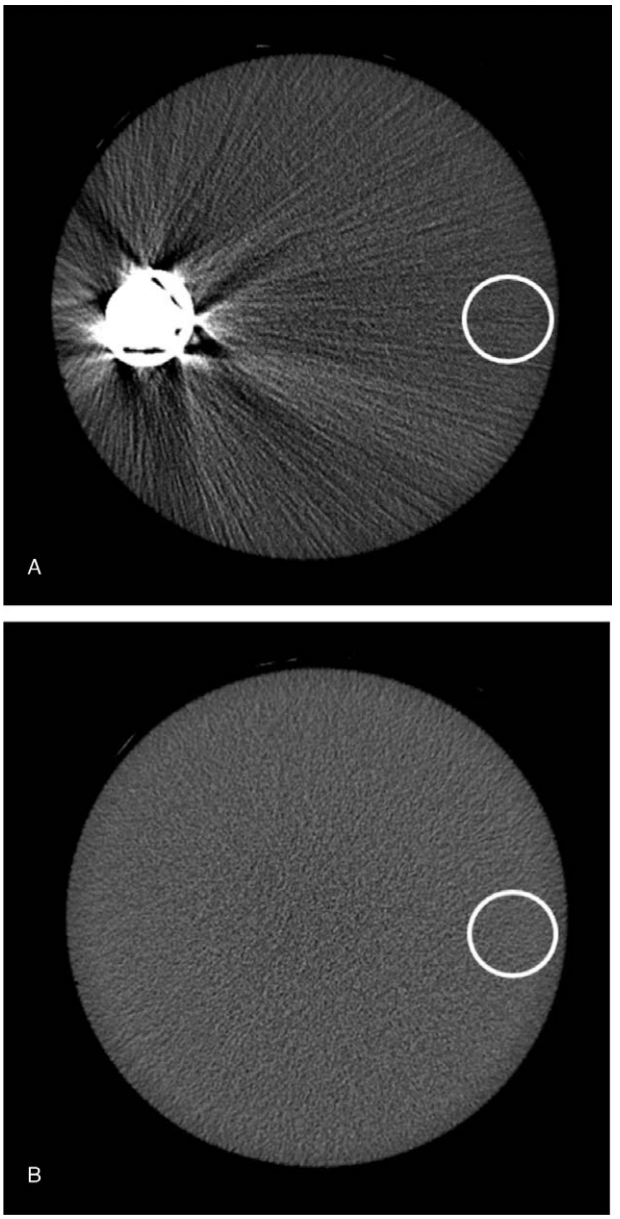

Figure 3. To calculate the difference in the standard deviations, a circular ROI was placed at the side opposite to the hip prosthesis to avoid the effects of the dark bands (A). An ROI was also placed in the same area in the phantom without the hip prosthesis (B) ROI = region of interest.

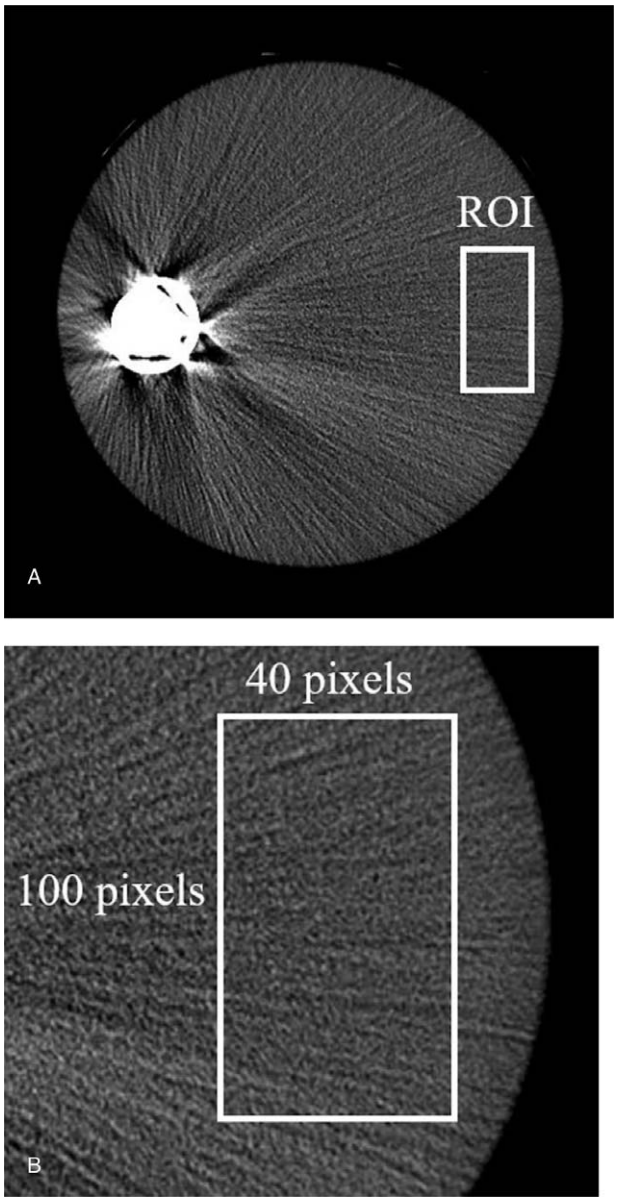

Figure 4. To calculate the location parameter of the Gumbel method for the assessment of fine streak artifacts, a rectangular ROI was placed at the opposite side of the hip prosthesis to avoid the effects of the dark bands (A). An ROI measuring 40 pixels in width and 100 pixels in length was placed almost perpendicular to the fine streak artifacts (B) ROI = region of interest.

the location parameter was calculated by:

$$\beta = b/a$$

and the location parameter was utilized as the index for the assessment of the fine streak artifacts.[12,13]

2.6. Statistical analysis

We used analyses of variance for statistical comparison of the extents and mean CT values of the dark bands, and of the difference in the SDs and location parameters of the fine streak artifacts. Furthermore, post hoc Scheffé tests was used to compare the parameters after the analysis of variance. A *P*-value of less than .05 was considered as being indicative of a statistically significant difference. Statistical analyses were performed using SPSS (SPSS statistics 25; IBM, Chicago, IL, US).

3. Results

3.1. Extent of the dark bands

The greatest reduction in the extent of the dark bands was observed in the images obtained by VMI at 140 keV with MAR, followed by VMI at 70 keV with MAR, conventional CT with MAR, VMI at 140 keV without MAR, conventional CT with MBIR, conventional CT with FBP and VMI at 70 keV without MAR (Table 1 and Fig. 5A). The dark bands were significantly reduced in each of the image sets reconstructed with MAR as compared to those that were not reconstructed with MAR (all, $P < .01$).

3.2. Mean CT values of the dark bands

The largest increase in the mean CT value of the dark bands was observed in the images obtained by VMI at 140 keV with MAR, followed by VMI at 70 keV with MAR, conventional CT with MAR, VMI at 140 keV without MAR, conventional CT with FBP, VMI at 70 keV without MAR and conventional CT with MBIR (Table 1 and Fig. 5B). The mean values were significantly increased in the images obtained by VMI at 140 keV with MAR and VMI at 70 keV with MAR as compared to the images not reconstructed with MAR (all, $P < .01$).

3.3. Difference in the SD of the fine streak artifacts

The difference in the SD of the fine streak artifacts showed the greatest degree of reduction in the images obtained by VMI at 140 keV with MAR, followed, in that order, by those obtained by conventional CT with MBIR, VMI at 140 keV without MAR, conventional CT with MAR, conventional CT with FBP, VMI at 70 keV without MAR and VMI at 70 keV with MAR (Table 1 and Fig. 5C). The fine streak artifacts were significantly reduced in each of the image sets obtained by VMI at 140 keV with/without MAR and conventional CT with MBIR as compared to the images obtained using other methods (all, $P < .05$), except that there were no differences between the images obtained by VMI at 140 keV without MAR and those obtained by conventional CT with MAR.

3.4. Location parameter for assessment of the fine streak artifacts

The greatest reduction in the location parameter estimated by the Gumbel method was observed in the images obtained by VMI at 140 keV with MAR, followed by VMI at 140 keV without MAR, conventional CT with MBIR, VMI at 70 keV with MAR, VMI at 70 keV without MAR, conventional CT with MAR and conventional CT with FBP (Table 1 and Fig. 5D). Significant reduction was observed in each of the images obtained by VMI at 140 keV with/without MAR and conventional CT with MBIR as compared to the images reconstructed by other methods (all, $P < .01$).

3.5. Images with each reconstruction

As mentioned above, the dark bands were reduced visually in images reconstructed with MAR as compared to the images not

Table 1

Results of quantitative evaluation of the artifacts in the images reconstructed using the different methods.

	Extent of the dark bands (mm^2)	Mean CT value of the dark bands (HU)	Difference in the SD of the fine streak artifacts (HU)	Location parameter of the fine streak artifacts
FBP	1684.8±137.2	−112.3±4.4	3.0±1.7	64.5±8.8
MAR	143.7±11.7	−99.9±4.3	2.6±0.7	54.5±3.5
MBIR	574.5±113.1	−141.7±16.8	0.9±0.5	29.2±1.1
VMI at 70 keV	1935.3±290.0	−126.9±8.4	3.3±0.6	43.4±2.2
VMI at 70 keV with MAR	47.6±36.3	−95.6±12.4	4.1±2.4	39.8±1.4
VMI at 140 keV	394.4±271.3	−104.1±8.4	1.6±0.4	26.4±1.7
VMI at 140 keV with MAR	18.3±12.0	−86.3±6.3	0.6±0.3	23.6±0.7

Data are represented as the averages±standard deviation.

CT = computed tomography, HU = hounsfield unit, SD = standard deviation, FBP = filtered back projection, MAR = metal artifact reduction, MBIR = model-based iterative reconstruction, VMI = virtual monochromatic imaging, keV = kilo-electron volts.

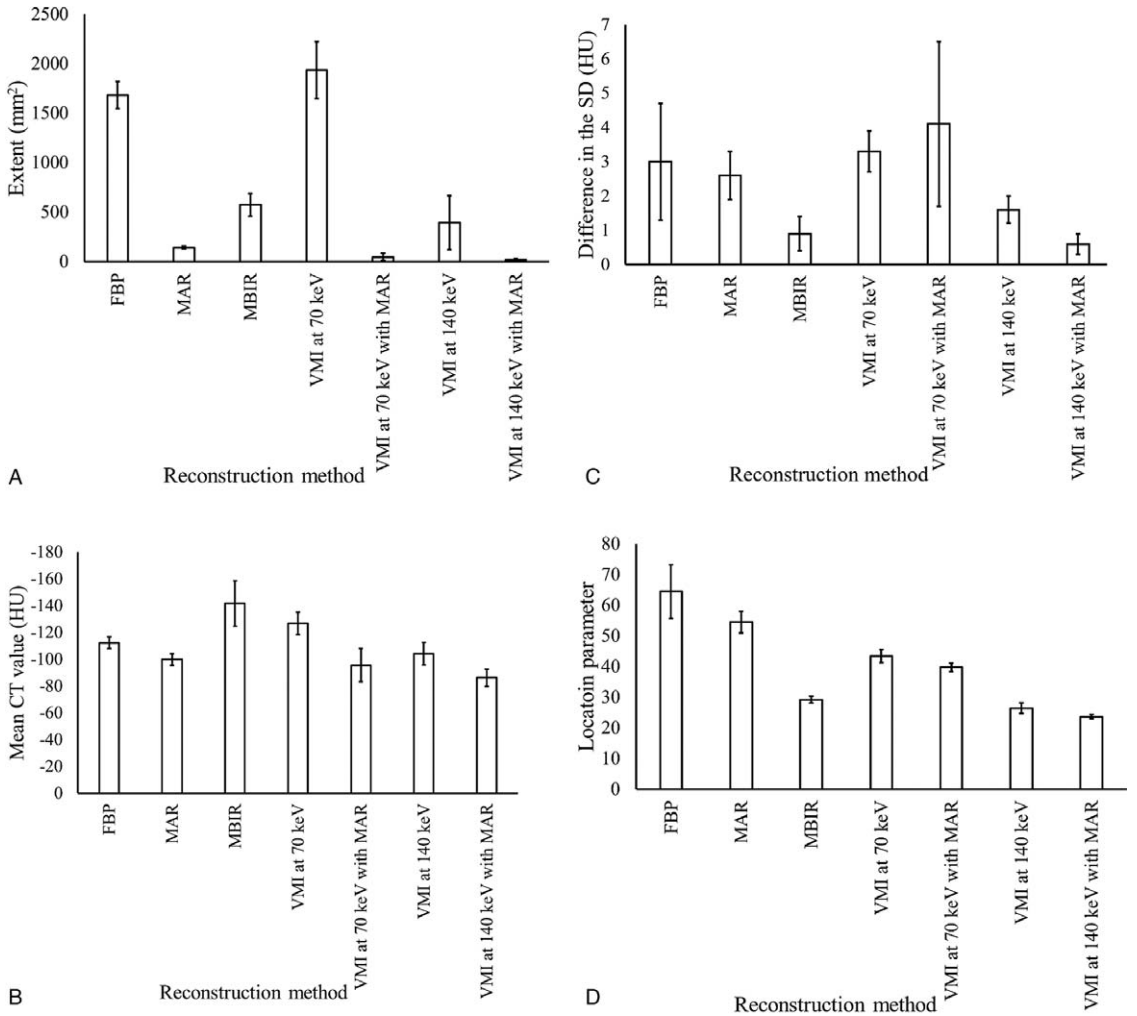

Figure 5. The extent of the dark bands was significantly reduced in each of the images reconstructed with MAR as compared to the images reconstructed without MAR (A). The mean CT value of the dark bands was significantly increased in the images obtained by VMI at 140 keV with MAR and VMI at 70 keV with MAR as compared to the images not reconstructed with MAR (B). As for fine streak artifacts, the differences in the SDs were significantly reduced in the images reconstructed by MBIR and images obtained by VMI at 140 keV with/without MAR, as compared to the images reconstructed by other methods, except that there were no differences between the images obtained by VMI at 140 keV and images obtained by conventional CT with MAR (C). Significant reduction of the location parameter was observed in the images reconstructed by MBIR and images obtained by VMI at 140 keV with/without MAR, as compared to the images reconstructed by other methods (D). CT = computed tomography, FBP = filtered back projection, HU = Hounsfield unit, keV = kilo-electron volts, MAR = metal artifact reduction, MBIR = model-based iterative reconstruction, SD = standard deviation, VMI = virtual monochromatic imaging.

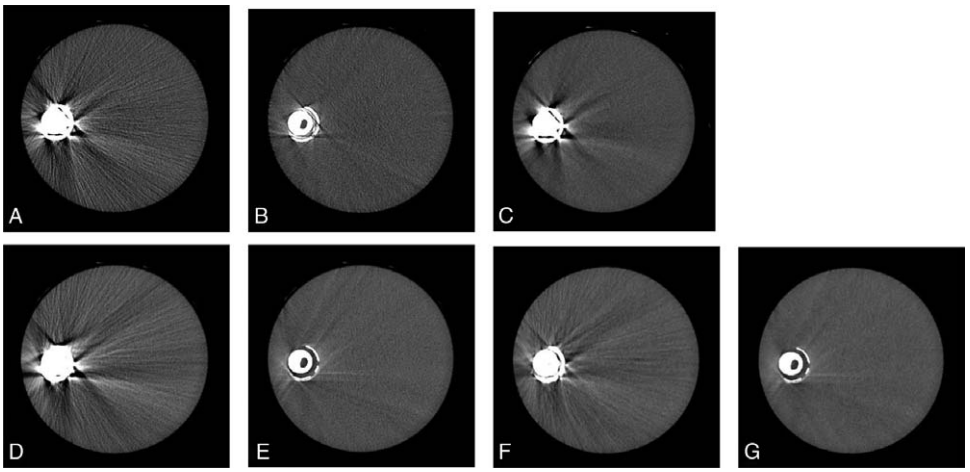

Figure 6. Dark bands were less noticeable in the images reconstructed with MAR as compared to those not reconstructed with MAR. Fine streak artifacts were less clear in the images reconstructed by MBIR and images obtained by VMI at 140 keV with/without MAR, as compared to the images reconstructed by other methods. A, FBP; B, MAR; C, MBIR; D, VMI at 70 keV; E, VMI at 70 keV with MAR; F, VMI at 140 keV; G, VMI at 140 keV with MAR. FBP = filtered back projection, keV = kilo-electron volts, MAR = metal artifact reduction, MBIR = model-based iterative reconstruction, VMI = virtual monochromatic imaging.

reconstructed with MAR (Fig. 6). Fine streak artifacts were less noticeable in the images obtained by VMI at 140 keV with/without MAR and conventional CT with MBIR (Fig. 6).

4. Discussion

Metal artifacts are caused by several reasons, such as beam hardening, photon starvation, and edge effect.[3,4,11,14–17] Beam hardening is caused by attenuation of low-energy photons when a polychromatic X-ray beam passes through an object. This results in an increase in the average energy of the beam and this phenomenon is called beam hardening. Beam hardening usually manifests as dark streaks in the CT images.[3,15–17] Photon starvation is generated by the absorption of a large proportion of photons during passage of a polychromatic beam through objects, resulting in an insufficient number of photons reaching the detector. This can generate thin dark and bright lines to appear alternately. These effects are particularly prominent when photons pass through high atomic number materials, such as metals, resulting in the generation of the so-called metal artifacts.[3,4] Edge effect is caused by the sharp edges of high atomic number materials, such as metal implants, which produces a high contrast as compared to adjacent structures. This effect manifests as tangential dark streaks to long straight edge.[14,16,17] Thus, metal artifacts can take various forms, caused by various combinations of the aforementioned phenomena. Beam hardening and edge effect are considered to manifest mainly as dark bands, while photon starvation manifests mainly as fine streak artifacts [3,14–17].

Thus, metal artifacts may have different appearances and be influenced by different factors, and each should be considered separately. Several quantitative indices have been reported to assess metal artifacts. As quantitative indices for dark bands, the area on the image with CT values lower than the threshold and the mean CT value of the area are frequently used.[2,6,7,18] Fine streak artifacts were evaluated objectively by using SD and artificial index, which was calculated using SD by placing an ROI within the fine streak artifacts[8,19,20]; however, the SD contained the effect of image noise and did not seem to reflect only metal artifacts. To remove the effect of image noise, it seems to be necessary to subtract SD of CT values within the ROI in the phantom without the metal implant from that in the phantom with the metal implant. Another evaluation method for fine streak artifacts is the Gumbel method devised by Imai et al.[12,13] The principle of the method is that the variations of the CT attenuation caused by fine streak artifacts can be statistically modeled by the Gumbel distribution. The largest difference between adjacent CT numbers of one CT number profile is attributed to fine streak artifacts.[12,13] Fine streak artifacts can be as reliably evaluated quantitatively by this method as by the differences in the SD; however, there are quite a few published articles reporting assessment of fine streak artifacts using the Gumbel method. In our study, we determined the extent of the low attenuation areas with CT values less than threshold and the mean CT values of the areas to evaluate dark bands, and the differences in the SDs and location parameters using the Gumbel method to evaluate fine streak artifacts, for comparing the usefulness of MAR, MBIR, and VMI for reducing metal artifacts in CT images.

In principle, MAR allows the corrupted data corresponding to the metal to be segmented and a new modified sinogram to be generated by correcting the original sinogram. In the first step, all pixels whose CT values are higher than the threshold are segmented as the metal, and a metal image is created. Then, the metal image is forward- projected to generate a metal sinogram. The corrupted data corresponding to the metal sinogram are then removed from the original uncorrected sinogram and the missing data are compensated for by interpolation of non-missing data obtained from the adjacent areas. Finally, the modified sinogram is created and back-projected to generate a corrected image with fewer metal artifacts.[5,21,22] In the process, phenomena such as beam hardening due to an absorption of low-energy photons during passage of the x-ray beam through metals, and the edge effect caused by sudden signal changes with high contrast seem to be suppressed, resulting in a decrease in the extent of dark bands. Articles have been published showing effectiveness of MARs, including algorithms from other vendors, to reduce dark bands. Based on a comparison of MARs and VMI, Neuhaus et al showed

the efficacy of VMI with MAR for orthopedic implants (Philips Healthcare, Amsterdam, Netherlands) and conventional CT at 120 kVp with MAR for orthopedic implants in reducing hypodense artifacts, in terms of the CT values and width, from hip prostheses as compared to VMI without MAR for orthopedic implants.[6] Higashigaito et al reported that use of iterative MAR (Siemens Healthcare, Forchheim, Germany) led to a more significant reduction of metal artifacts including dark bands than VMI without MAR.[23] In comparing MARs with MBIR, Angeliki et al showed that iterative MAR allowed significant reduction of metal artifacts, including dark streaks, as compared to advanced modeled iterative reconstruction (ADMIRE; Siemens).[7] Yasaka et al reported that single-energy MAR (Canon Medical Systems, Ohtawara, Japan) significantly reduced metal artifacts, including dark streaks, as compared to a forward-projected MBIR solution (Canon Medical Systems).[24] In our study, MAR showed significant efficacy in reducing dark bands as compared to other methods of reconstruction. The aforementioned results from previous studies demonstrating the effectiveness of MAR in reducing dark bands are consistent with our findings, although, to the best of our knowledge, no study until date has compared MAR, MBIR, and VMI to determine which might be the most effective for reducing only dark bands among several kinds of metal artifacts. In this study, we initially showed that among the image reconstruction methods, MAR was the most effective for reducing dark bands. In addition, MAR also showed some effect in reducing fine streak artifacts. Fine streak artifacts were fewer in images reconstructed with MAR than those reconstructed by FBP, in images obtained by VMI at 70 keV with MAR than in those obtained by VMI at 70 keV without MAR, and in images obtained by VMI at 140 keV with MAR than in those obtained by VMI at 140 keV without MAR. However, the capability of MAR to suppress fine streak artifacts was inferior to that of MBIR or VMI at 140 keV. MAR yielded the most promising results for dark bands reduction, as mentioned above, while some reports have pointed out some disadvantages of MAR. MAR has been shown to cause a distortion in the shapes of metal implants and lead to an underestimation of their size.[25–27] Lee et al showed that the thickness of the titanium was underestimated in images obtained by VMI at 140keV with MAR.[26] In another report by Wang et al, images obtained with MAR showed an unacceptable distortion in the shape and size of a pedicle screw.[27] Furthermore, MAR also seems to introduce new artifacts.[7,22,28]

MBIR is a fully iterative reconstruction algorithm that does not involve blending with FBP images. The feature of this technology is to mathematically model information about various parameters, such as the X-ray focal spot size, the shape and size of the X-ray detector, and the geometric information of the X-ray passing through the metal, digitize them, and incorporate them into the calculation process. It measures how much error there is between the raw data actually obtained and the virtual raw data projected from the image, and minimizes this difference during the image reconstruction.[20,24,29,30] In the process, photon starvation seems to be corrected, resulting in a reduction of low signal artifacts which appear as fine streak artifacts in CT images.[4,29,30] The ability of MBIR to reduce fine streak artifacts has been reported previously. Katsura et al showed that MBIR significantly reduced fine streak artifacts in the cervicothoracic region, as compared to adaptive iterative reconstruction (GE healthcare) and FBP.[8] Similar results were reported by Kuya et al, who showed the effectiveness of MBIR for reduction of fine streak artifacts generated from dental hardware.[20] However, to the best of our knowledge, no previous study has compared the effectiveness of MAR, MBIR, and VMI in reducing fine streak artifacts. In our comparison of the 3 methods in the present study, MBIR was found to be the most effective in decreasing fine streak artifacts as compared to the other image reconstruction methods, except for VMI at 140 keV with/without MAR. On the other hand, MBIR did not show promising effect in reducing dark bands, probably because MBIR does not seem to be so effective for suppressing phenomena such as beam hardening and edge effect, which seemed to be the main causes of the dark bands.

VMI obtained by dual-energy CT yields images that appear to be obtained with a monochromatic beam, and can be reconstructed over a wide range of keV levels. The image contrast is higher in images reconstructed at lower keV values, lower in images reconstructed at higher keV values.[5,31] Since beam hardening artifacts are caused by a polychromatic X-ray beam, VMI, especially at higher keV, is principally useful to correct beam hardening artifacts, which seem to be the main cause of dark bands.[5,19,31,32] In our study, images obtained by VMI at 140 keV showed the greatest reduction among the images not reconstructed with MAR, and images obtained by VMI at 140 keV with MAR showed the greatest reduction among the images obtained with MAR, although the difference was not significant. Images obtained by VMI at 140 keV showed some reduction of dark bands, however, the effectiveness of VMI at 140 keV was inferior to that of MAR. As for VMI at 70 keV, its capability of decreasing dark bands was inferior, in terms of both the extent and the mean CT value, to the use of FBP for image reconstruction. On the other hand, images obtained by VMI at 140 keV with/without MAR showed significant improvement in reducing fine streak artifacts as compared to images obtained using other reconstruction methods, except for MBIR. One of the main reasons for these results is speculated as follows: the contrast of the images is decreased in images obtained by VMI at 140 keV with/without MAR. The contrast of the fine streak artifacts, which consist of thin lines alternately showing low and high attenuation also seems to be reduced and the artifacts seem to be obscured in the images. The feasibility of reducing fine streak artifacts by VMI at high energy levels has been reported in the past. Lewis et al showed that images obtained by VMI at 150 keV showed the greatest reduction of fine streak artifacts among several energy levels used.[33] Dong et al demonstrated that VMI at high energy levels, especially 120 keV, was effective for reducing metal artifacts, including fine streak artifacts.[19] However, as mentioned above, to the best of our knowledge, no previous reports have evaluated which of the reconstruction methods may be the best choice for decreasing fine streak artifacts. Here, we report for the first time, that images obtained by VMI at 140 keV with/without MAR showed prominent reduction of fine streak artifacts. However, a disadvantage in images obtained by VMI at 140 keV with/without MAR seems to be that the contrast of the soft tissue structures adjacent to the metal implants is decreased, in addition to the reduction of the fine streak artifacts, and that structures are obscured by the high energy level used.[34]

Furthermore, the effectiveness of a combination of MARs and VMI has also been reported. Neuhaus et al showed that the combination of MAR for orthopedic implants and VMI yielded significant reduction of hypodense and hyperdense artifacts caused by hip prostheses, compared to other techniques.[6] Dong

et al demonstrated the effectiveness of the combination with VMI at 120 keV or 140 keV for reduction of metal artifacts in patients with a unilateral hip prosthesis.[35] In our study, images obtained using MAR showed marked reduction, and those obtained by VMI at 140 keV showed mild reduction of dark bands, as mentioned above. As a result, images obtained by VMI at 140 keV with MAR showed the greatest reduction, followed by images obtained by VMI at 70 keV with MAR, although the difference was not significant. As for fine streak artifacts, images obtained by VMI at 140 keV with MAR showed the greatest reduction of fine streak artifacts, while there was no significant difference from the images obtained by VMI at 140 keV without MAR. Thus, the combination of MAR and VMI at 140 keV was more effective in reducing both dark bands and fine streak artifacts than the use of either method, although the synergistic effects were not so strong as to yield a significant difference as compared to the effect obtained using either one of the methods.

This study had several limitations. First, we only assessed metal artifacts quantitatively and did not perform visual evaluation. Further subjective evaluation is preferable to confirm the quantitative results. Second, we did not conduct clinical evaluations of the patients with metal implants; the usefulness of the reconstruction methods also needs to be validated in a clinical study. Third, we only evaluated metal artifacts in a phantom study using a unilateral hip prosthesis made of titanium. The capability of the methods to reduce metal artifacts caused by bilateral hip prostheses and other types of metal implants for the other body parts also needs to be discussed. Fourth, our study was vendor-specific and the CT scanner and reconstruction algorithms that we used in this study were from a single vendor. Differences in the image reconstruction algorithms used by the other vendors could influence the results. Fifth, we did not evaluate the metal artifacts in the images obtained with the changed scanning parameters including milliampere-second. Changing the parameters can affect the appearance of the metal artifacts. Sixth, we did not assess the distortion in the shape and underestimation in the size of the metal implants and the new artifacts caused by MAR, as reported in previous studies.[7,22,25–28] Lastly, our study did not assess the appearance of the structures adjacent to the metal implants obscured by the metal artifacts.

In conclusion, the effectiveness of MAR, MBIR, and VMI in reducing metal artifacts would depend on the type of the artifacts. For metal artifacts arising from a unilateral hip prosthesis, MAR appears to be the most suitable image reconstruction method to reduce dark bands, and MBIR and VMI at 140 keV appear to be markedly effective for reducing fine streak artifacts.

Author contributions

Conceptualization: Takuya Ishikawa.
Data curation: Takuya Ishikawa.
Formal analysis: Shingo Harashima.
Investigation: Rika Fukui.
Methodology: Masafumi Kaiume.
Project administration: Shigeru Suzuki.
Software: Shingo Harashima.
Supervision: Shigeru Suzuki.
Validation: Yoshiaki Katada.
Visualization: Takuya Ishikawa.
Writing – original draft: Takuya Ishikawa.

References

[1] Roth TD, Maertz NA, Parr JA, et al. CT of the hip prosthesis: appearance of components, fixation, and complications. Radiographics 2012;32: 1089–107.
[2] Bamberg F, Dierks A, Nikolaou K, et al. Metal artifact reduction by dual energy computed tomography using monoenergetic extrapolation. Eur Radiol 2011;21:1424–9.
[3] Franz EB, Dominik F. CT artifacts: causes and reduction techniques. Imaging Med 2012;4:229–40.
[4] Barrett JF, Keat N. Artifacts in CT: recognition and avoidance. Radiographics 2004;24:1679–91.
[5] Bhavik NP, Daniele M. Strategies to improve image quality on dual-energy computed tomography. Radiol Clin N Am 2018;56:641–7.
[6] Neuhaus V, Grosse HN, Zopfs D, et al. Reducing artifacts from total hip replacements in dual layer detector CT: combination of virtual monoenergetic images and orthopedic metal artifact reduction. Eur J Radiol 2019;111:14–20.
[7] Angeliki N, Steve PM, Ilias B, et al. Metallic artifact reduction by evaluation of the additional value of iterative reconstruction algorithms in hip prosthesis computed tomography imaging. Medicine 2019;98:e14341.
[8] Katsura M, Sato J, Akahane M, et al. Comparison of pure and hybrid iterative reconstruction techniques with conventional filtered back projection: image quality assessment in the cervicothoracic region. Eur J Radiol 2013;82:356–60.
[9] Chou R, Chi HY, Lin YH, et al. Comparison of quantitative measurements of four manufacturer's metal artifact reduction techniques for CT imaging with a self-made acrylic phantom. Technol Health Care 2020;28:273–87.
[10] Kesong Z, Qing H, Xiaolin X, et al. Metal artifact reduction of orthopedics metal artifact reduction algorithm in total hip and knee arthroplasty. Medicine 2020;99:e19268.
[11] Iman K, Amanda I, Elliot KF, et al. Metal about the hip and artifact reduction techniques: from basic concepts to advanced imaging. Semin Musculoskelet Radiol 2019;23:e68–81.
[12] Imai K, Ikeda M, Kawaura C, et al. Dose reduction and image quality in CT angiography for cerebral aneurysm with various tube potentials and current settings. Br J Radiol 2012;85:673–81.
[13] Imai K, Ikeda M, Enchi Y, et al. Quantitative assessment of image noise and streak artifacts on CT image: Comparison of z-axis automatic tube current modulation technique with fixed tube current technique. Comput Med Imaging Graph 2009;33:353–8.
[14] Schulze R, Heil U, Gross D, et al. Artefacts in CBCT: a review. Dentomaxillofac Radiol 2011;40:265–73.
[15] Abhishek S, Anuj M, Sunita S, et al. Understanding artifacts in cone beam computed tomography. Int J Maxillofac Imaging 2016;2:51–4.
[16] Anil KN, Neha D, Rana T. Artifacts: the downturn of CBCT image. J Int Soc Prev Community Dent 2015;5:440–5.
[17] De Man B, Nuyts J, Dupont P, et al. Metal streak artifacts in X-ray computed tomography: a simulation study. IEEE T Nucl Sci 1999;46:691–6.
[18] Filograna L, Magarelli N, Leone A, et al. Performances of low-dose dual-energy CT in reducing artifacts from implanted metallic orthopedic devices. Skeletal Radiol 2016;45:937–47.
[19] Dong Y, Shi AJ, Wu JL, et al. Metal artifact reduction using virtual monochromatic images for patients with pedicle screws implants on CT. Eur Spine J 2016;25:1754–63.
[20] Kuya K, Shinohara Y, Kato A, et al. Reduction of metal artifacts due to dental hardware in computed tomography angiography: assessment of the utility of model-based iterative reconstruction. Neuroradiology 2017;59:231–5.
[21] Alain B, Meyer JB, Raymond A, et al. CT of hip prosthesis: new techniques and new paradigms. Diagn Interv Imaging 2016;97:725–33.
[22] Katsura M, Sato J, Akahane M, et al. Current and novel techniques for metal artifact reduction at CT: practical guide for radiologists. Radiographics 2018;38:450–61.
[23] Higashigaito K, Angst F, Runge VM, et al. Metal artifact reduction in pelvic computed tomography with hip prostheses: comparison of virtual monoenergetic extrapolations from dual-energy computed tomography and an iterative metal artifact reduction algorithm in a phantom study. Invest Radiol 2015;50:828–34.
[24] Yasaka K, Kamiya K, Irie R, et al. Metal artefact reduction for patients with metallic dental fillings in helical neck computed tomography: comparison of adaptive iterative dose reduction 3D (AIDR 3D), forward-projected model-based iterative reconstruction solution (FIRST) and AIDR 3D with single-energy metal artefact reduction (SEMAR). Dentomaxillofac Radiol 2016;45:20160114.

[25] Huang JY, Kerns JR, Nute JL, et al. An evaluation of three commercially available metal artifact reduction methods for CT imaging. Phys Med Biol 2015;60:1047–67.
[26] Lee YH, Park KK, Song HT, et al. Metal artefact reduction in gemstone spectral imaging dual-energy CT with and without metal artefact reduction software. Eur Radiol 2012;22:1331–40.
[27] Wang Y, Qian B, Li B, et al. Metal artifacts reduction using monochromatic images from spectral CT: evaluation of pedicle screws in patients with scoliosis. Eur J Radiol 2013;82:360–6.
[28] Han SC, Chung YE, Lee YH, et al. Metal artifact reduction software used with abdominopelvic dual-energy CT of patients with metal hip prostheses: assessment of image quality and clinical feasibility. Am J Roentgenol 2014;203:788–95.
[29] Corey TJ, Morgan ET, Nicolaus AW, et al. Evaluation of abdominal CT image quality using a new version of vendor-specific model-based iterative reconstruction. J Comput Assist Tomogr 2017;4:67–74.
[30] Telesmanich ME, Jensen CT, Enriquez JL, et al. Third version of vendor-specific model-based iterative reconstruction (Veo 3.0): evaluation of CT image quality in the abdomen using new noise reduction presets and varied slice optimization. Br J Radiol 2017;90:20170188.
[31] Kai RL, Simon L, Victor FN, et al. CT metal artifacts in patients with total hip replacements: for artifact reduction monoenergetic reconstructions and post-processing algorithms are both efficient but not similar. Eur Radiol 2018;28:4524–33.
[32] Victor N, Nils GH, Nuran A, et al. Metal artifact reduction by dual-layer computed tomography using virtual monoenergetic images. Eur J Radiol 2017;93:143–8.
[33] Lewis M, Reid K, Toms AP. Reducing the effects of metal artefact using high keV monoenergetic reconstruction of dual energy CT (DECT) in hip replacements. Skeletal Radiol 2013;42:275–82.
[34] De CA, Casselman J, Van HT, et al. Analysis of metal artifact reduction tools for dental hardware in CT scans of the oral cavity: kVp, iterative reconstruction, dual-energy CT, metal artifact reduction software: does it make a difference? Neuroradiology 2015;57:841–9.
[35] Dong Y, Cheng FR, Cai N, et al. Reduction of metal artifacts from unilateral hip arthroplasty on dual-energy CT with metal artifact reduction software. Acta Radiol 2018;59:853–60.